

Fixed-time Disturbance Observer-Based MPC Robust Trajectory Tracking Control of Quadrotor

Liwen Xu, Bailing Tian, Cong Wang, Junjie Lu, Dandan Wang, Zhiyu Li, Qun Zong

Abstract—In this paper, a fixed-time disturbance observer-based model predictive control algorithm is proposed for trajectory tracking of quadrotor in the presence of disturbances. First, a novel multivariable fixed-time disturbance observer is proposed to estimate the lumped disturbances. The bi-limit homogeneity and Lyapunov techniques are employed to ensure the convergence of estimation error within a fixed convergence time, independent of the initial estimation error. Then, an observer-based model predictive control strategy is formulated to achieve robust trajectory tracking of quadrotor, attenuating the lumped disturbances and model uncertainties. Finally, simulations and real-world experiments are provided to illustrate the effectiveness of the proposed method.

Index Terms—Trajectory Tracking Control, Fixed-Time Disturbance Observer, Model Predictive Control, Quadrotor UAV.

I. INTRODUCTION

QUADROTOR Unmanned Aerial Vehicles (UAVs) have been utilized in diverse fields such as aerial delivery, inspection, rescue, and surveillance, owing to their remarkable capabilities, which include vertical take-off and landing, autonomous flight, and mapping [1], [2]. However, the control performance of quadrotor can be significantly affected by model uncertainty, aerodynamic drag force, and external disturbances, such as wind gusts and payloads with unknown mass. To ensure the safety and high performance of quadrotor in such scenarios, it is crucial to improve the trajectory tracking capability of quadrotor, especially in the presence of disturbances.

In recent years, numerous control methods have been proposed for trajectory tracking of quadrotor, which can be broadly categorized into linear control methods and nonlinear control methods. Linear control methods, such as classical PID [3], [4] and linear quadratic regulator [5], [6], are relatively straightforward to implement and comprehend. Specifically, in [4], a PID-based controller that depends on the system model is proposed, providing exponential stability for the attitude system of quadrotor. However, due to the high nonlinear



Fig. 1. Trajectory visualization utilizing the proposed FxTDO-MPC algorithm in real-world experiments. More details can be found in the attached video at <https://youtu.be/O4BDXRdd0Do> or <https://www.bilibili.com/video/BV11h4y1i7oF/>.

dynamics and strong coupling of quadrotor, nonlinear methods exhibit more potential to achieve outstanding performance, such as sliding mode control [7]–[9], backstepping control [10], [11], incremental nonlinear dynamic inversion (INDI) [12], [13], active disturbance rejection control [14] and neural networks-based control [15]. On the other hand, the combination of different methods can significantly enhance the control performance of quadrotor. For instance, in [9], an adaptive method employed in the outer loop is integrated with a sliding mode control method employed in the inner loop, leading to substantial enhancement in robustness. In spite of the extensive development of robust techniques, the model predictive control (MPC) is widely acknowledged as a crucial tool for UAV control systems. The MPC method, by applying optimal control techniques within a specific context, adeptly addresses complex tasks through simultaneous consideration of multiple constraints and objectives via optimization. There are existing literature on the application of MPC with disturbance estimation for quadrotor. In [16], [17], a model predictive controller is proposed for position control of quadrotor. Additionally, augmented-state Kalman Filter disturbance estimators are designed to accurately estimate disturbances. In [18], a Gaussian Process method is utilized to model aerodynamic effect disturbances of quadrotor. However, offline learning procedure reduces the robustness and real-time performance of the controller. In [19], [20], deep neural network-based methods are employed to predict disturbances and provide disturbance information for MPC. However, the effect relies on the training procedure and exhibits limited resilience to variations in the environment. In addition to the disturbance estimation methods mentioned above, some sliding mode disturbance observer techniques are integrated into the MPC

This work was supported in part by the National Natural Science Foundation of China under Grants 62273249, 62203415, 62373268, 62022060, 52304170, and 62373273. (Corresponding author: Zhiyu Li.)

Liwen Xu, Bailing Tian, Junjie Lu, Zhiyu Li and Qun Zong are with the Tianjin Key Laboratory of Intelligent Unmanned Swarm Technology and System, School of Electrical and Information Engineering, Tianjin University, Tianjin 300072, China (e-mail: xlw_2000@tju.edu.cn; bailing_tian@tju.edu.cn; lqzx1998@tju.edu.cn; lizhiyu@tju.edu.cn; zongqun@tju.edu.cn)

Cong Wang is with the College of Field Engineering, Army Engineering University of PLA, 210007, Nanjing, China (e-mail: lgd_dolphin@139.com)

Dandan Wang is with Beijing Tianma Intelligent Control Technology Co., Ltd. Beijing 101399, China (e-mail: dandanwang0910@163.com)

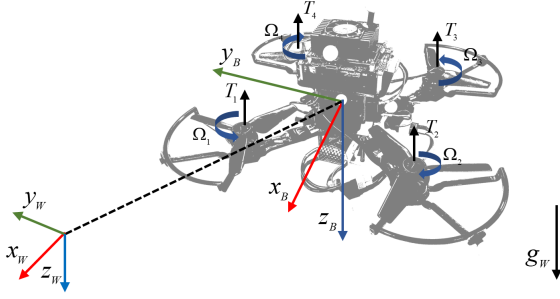


Fig. 2. Quadrotor model with World frame W and Body frame B . T_i and Ω_i are respectively single thrust and speed of the individual rotors.

framework. In [21], a finite-time sliding mode observer is employed within a robust model predictive control framework to estimate the additive disturbance for perturbed continuous-time systems. In [22], a sliding mode disturbance observer is developed to estimate the lumped disturbances, which are then utilized by MPC for underwater-vehicle manipulators systems. Moreover, it has been shown that the convergence rate of disturbance observer plays an important role in constructing observer-based MPC control system [23], [24].

Motivations: In summary, the quadrotor is a strongly coupled and underactuated nonlinear system. It is challenging to achieve satisfactory performance using linear control methods for quadrotor [5], [6]. In contrast, model predictive control (MPC), as a nonlinear optimization method, can effectively address the coupled multivariable nonlinear control problems by considering prediction model constraint. However, the success of MPC depends on the availability of a highly accurate prediction model [17]–[20], [23]. Therefore, the rapid provision of such an accurate model is an urgent problem to be solved [18], [19]. Motivated by these observations, a novel fixed-time disturbance observer (FxTDO) is proposed to accurately estimate the lumped disturbances with fast convergence. Subsequently, by integrating the estimation from the FxTDO with the nominal model, the FxTDO-based MPC (FxTDO-MPC) algorithm is developed to achieve robust trajectory tracking of quadrotor in the presence of disturbances. Fig. 1 shows the trajectory of quadrotor utilizing the proposed FxTDO-MPC algorithm in real-world experiments. The main contributions of this paper can be summarized in the following two aspects.

- 1) A novel multivariable FxTDO is proposed to estimate the lumped disturbances, and the bi-limit homogeneity and Lyapunov techniques are employed to ensure the convergence of estimation error within a fixed convergence time, independent of the initial estimation error.
- 2) By integrating the disturbance observations into the prediction model within the MPC framework, an FxTDO-MPC algorithm is developed to achieve robust trajectory tracking of quadrotor. Simulations and real-world experiments are presented to validate the effectiveness of the proposed algorithm.

The rest of this paper is organized as follows. In Section II, the dynamics of quadrotor and control objective are provided. The design of the FxTDO-MPC algorithm is introduced in Section III. In Section IV, the results of simulations in Gazebo and real-world experiments are presented. Finally, Section V

concludes this paper.

II. MODEL AND CONTROL OBJECTIVE STATEMENT

To describe the dynamics of quadrotor, two frames are defined: the World frame, denoted as W , and the Body frame, denoted as B , as illustrated in Fig. 2. The subscript of the variable i.e. $\{x_W, y_W, z_W\}$, indicates the specific frame where the variable is defined. x_W, y_W, z_W point north, east and down, and x_B, y_B, z_B point forward, right and down. Unless necessary, the subscript representing the coordinate frame is dropped throughout the paper for notational convenience. The frame W is fixed on the ground. The frame B is located at the center of mass of quadrotor. Four rotors, lying on the xy -plane of frame B , generate individual thrust (T_1 - T_4) perpendicular to the xy -plane.

The model of quadrotor is defined as a rigid body with 6 degree-of-freedom (DoF). The dynamics of quadrotor can be described by:

$$\dot{\mathbf{p}} = \mathbf{v}, \quad (1a)$$

$$\dot{\mathbf{v}} = -\frac{1}{m} \mathbf{R}_B^W(q) T_c \mathbf{e}_z^B + \mathbf{g} + \frac{1}{m} \mathbf{f}_d, \quad (1b)$$

$$\dot{\mathbf{q}} = \frac{1}{2} \mathbf{q} \otimes \begin{bmatrix} 0 \\ \boldsymbol{\omega} \end{bmatrix}, \quad (1c)$$

$$\dot{\boldsymbol{\omega}} = \mathbf{J}^{-1} [\boldsymbol{\tau}_c - \boldsymbol{\omega} \times \mathbf{J} \boldsymbol{\omega}] + \mathbf{J}^{-1} \boldsymbol{\tau}_d, \quad (1d)$$

where $\mathbf{p} = [p_x, p_y, p_z]^T \in \mathbb{R}^3$ and $\mathbf{v} = [v_x, v_y, v_z]^T \in \mathbb{R}^3$ are respectively position and velocity vectors of center of mass in the frame W . The symbol T represents the transpose. Unit quaternions, denoted as $\mathbf{q} = [q_w, q_x, q_y, q_z]^T \in \mathbb{R}^4$ and satisfying $\|\mathbf{q}\| = 1$, represent the orientation of quadrotor in the frame W . $\boldsymbol{\omega} = [\omega_x, \omega_y, \omega_z]^T \in \mathbb{R}^3$ is angular velocity in the frame B , m is the quadrotor mass, and $\mathbf{g} = [0, 0, 9.81m/s^2]^T$ denotes gravity vector in the frame W . $\mathbf{J} \in \mathbb{R}^{3 \times 3}$ is inertia matrix. The operator \times represents the cross product. The vector $\mathbf{f}_d \in \mathbb{R}^3$ represents the lumped disturbance, which is caused by aerodynamic drag force and external disturbances, such as wind gusts and unknown payloads. The vector $\boldsymbol{\tau}_d \in \mathbb{R}^3$ represents unknown torque disturbance arising from inaccurate inertia matrix and external disturbances. $\mathbf{R}_B^W(q) \in \text{SO}(3)$ denotes rotation matrices from frame B to frame W :

$$\mathbf{R}_B^W(q) = \begin{bmatrix} 1-2q_y^2-2q_z^2 & 2(q_xq_y-q_wq_z) & 2(q_wq_y+q_xq_z) \\ 2(q_xq_y+q_wq_z) & 1-2q_x^2-2q_z^2 & 2(q_yq_z-q_wq_x) \\ 2(q_xq_z-q_wq_y) & 2(q_wq_x-q_yq_z) & 1-2q_x^2-2q_y^2 \end{bmatrix}. \quad (2)$$

Additionally, $T_c \in \mathbb{R}$ and $\boldsymbol{\tau}_c = [\tau_x, \tau_y, \tau_z]^T \in \mathbb{R}^3$, as (4) shows, are respectively the collective thrust command and the body torque command generated from four rotors. $\mathbf{e}_z^B = [0, 0, 1]^T$ means z -direction of the frame B . Consequently, $\mathbf{R}_B^W(q) T_c \mathbf{e}_z^B$ means rotating $[0, 0, T_c]$ from the frame B to the frame W . Operator \otimes is defined as:

$$\mathbf{q} \otimes \begin{bmatrix} 0 \\ \boldsymbol{\omega} \end{bmatrix} = \begin{bmatrix} 0 & -\omega_x & -\omega_y & -\omega_z \\ \omega_x & 0 & \omega_z & -\omega_y \\ \omega_y & -\omega_z & 0 & \omega_x \\ \omega_z & \omega_y & -\omega_x & 0 \end{bmatrix} \mathbf{q}. \quad (3)$$

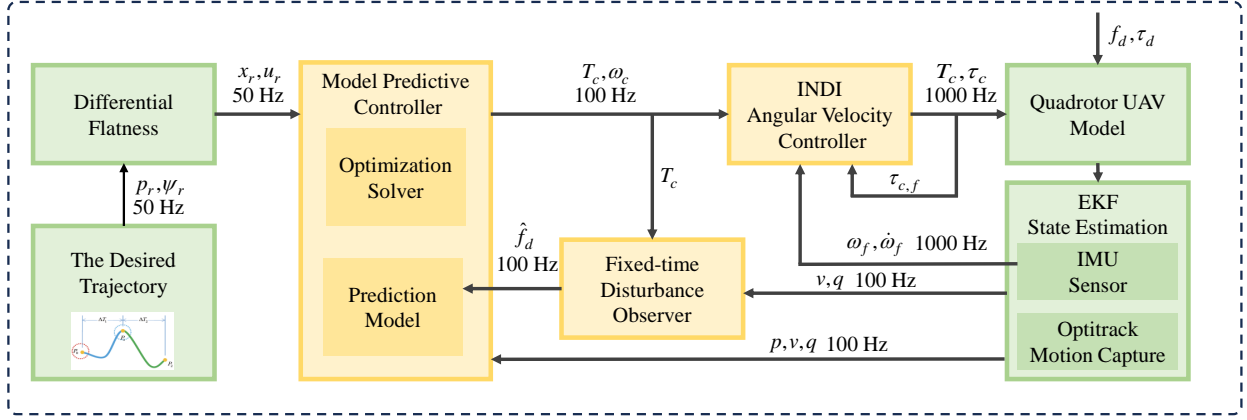


Fig. 3. System overview of the proposed algorithm applied to quadrotor system. The frequencies of MPC and FxTDO are decided based on the computational time of FxTDO-MPC running on the onboard computer. Besides, the frequency of INDI angular velocity controller is selected based on the PX4 Autopilot User Guide. Additionally, the generating frequency of the desired trajectory is chosen to cooperate with the controller.

Finally, T_c and τ_c can be computed based on the single thrust of each rotor:

$$T_c = \sum T_i \quad , \quad \tau_c = \begin{bmatrix} d_y(-T_0 - T_1 + T_2 + T_3) \\ d_x(-T_0 + T_1 + T_2 - T_3) \\ c_\tau(-T_0 + T_1 - T_2 + T_3) \end{bmatrix}, \quad (4)$$

where d_x, d_y are the rotor displacements and c_τ is the rotor drag torque constant.

The main objective of the presented work is to develop a fixed-time disturbance observer-based MPC methodology that computes appropriate T_c and τ_c to accurately track the desired trajectory while effectively compensating for disturbances. To achieve the control objectives, the following assumption is required.

Assumption 1: Suppose that the lumped disturbance vector \mathbf{f}_d in (1b) is continuous differentiable, and there exist some positive constants δ and $\bar{\delta}$ such that $\|\mathbf{f}_d\| \leq \delta$ and $\|\dot{\mathbf{f}}_d\| \leq \bar{\delta}$.

III. DESIGN OF FXTDO-MPC ALGORITHM AND INDI ANGULAR VELOCITY CONTROLLER

In this section, an FxTDO-MPC algorithm is proposed. First, an FxTDO is designed to estimate the lumped disturbances. Then, a model predictive controller is developed to track the desired trajectory while compensating for the lumped disturbances. Finally, an INDI angular velocity controller is adopted to deal with unknown torque disturbance. The architecture of the integrated controller and observer is provided in Fig. 3.

A. Related Lemmas

Lemma 1: [25] Let $\eta : \mathbb{R}^n \rightarrow \mathbb{R}$ and $\gamma : \mathbb{R}^n \rightarrow \mathbb{R}_+$ be two upper semicontinuous, single-valued bi-homogeneous functions, with the same weights, degrees and approximating functions. Suppose that $\forall x \in \mathbb{R}^n, \{x \in \mathbb{R}^n \setminus \{0\} : \gamma(x) = 0\} \subseteq \{x \in \mathbb{R}^n \setminus \{0\} : \eta(x) < 0\}$. Then, there exists a real number λ^* such that, for all $\lambda \geq \lambda^*$, $\eta(x) - \lambda\gamma(x) < 0$.

Lemma 2: [25] Consider a homogeneous in the bi-limit set-valued vector field $\mathbf{f} : \mathbb{R}^n \rightarrow \mathbb{R}^n$, which is upper semicontinuous, with associated triples $(\mathbf{r}_0, k_0, \mathbf{f}_0)$ and $(\mathbf{r}_\infty, k_\infty, \mathbf{f}_\infty)$

such that the origins of the system (5) are globally asymptotically stable equilibria. Let m_0 and m_∞ be real numbers such that $m_0 > \max\{r_i^0\}$ and $m_\infty > \max\{r_i^\infty\}$. Then there exists a C^1 , positive definite function $V(\mathbf{x})$ such that the derivative of $V(\mathbf{x})$ is bi-homogeneous and negative definite. Moreover, if $k_0 \leq k_\infty$ there exist positive constants $\kappa_0 > 0$ and $\kappa_\infty > 0$ such that the inequality hold for all $\mathbf{x} \in \mathbb{R}^n$, $\dot{V}(\mathbf{x}) \leq -\kappa_0 V^{\frac{m_0+k_0}{m_0}}(\mathbf{x}) - \kappa_\infty V^{\frac{m_\infty+k_\infty}{m_\infty}}(\mathbf{x})$.

B. Fixed-Time Disturbance Observer Design

Firstly, an FxTDO is introduced to estimate the lumped disturbance \mathbf{f}_d in (5), guaranteeing the convergence of the estimation error within a fixed time T, i.e., the estimation error converges globally in finite time, and the convergence time is globally bounded by a positive constant T, independent of the initial estimation error [26]. Consider the quadrotor dynamics (1b), which can be rewritten as the following multivariable first-order system:

$$\dot{\mathbf{z}}_1 = \mathbf{T} + \mathbf{f}_d, \quad (5)$$

where $\mathbf{z}_1 = m\mathbf{v}$, $\mathbf{T} = m\mathbf{g} - \mathbf{R}_B^W(q)T_c \mathbf{e}_z^B$ is the virtual control input. Inspired by our previous work in [27], by including a discontinuous term $[\mathbf{e}_1]^0$, the following improved observer is designed to estimate the lumped disturbance \mathbf{f}_d .

$$\begin{aligned} \dot{\hat{\mathbf{z}}}_1 &= \hat{\mathbf{f}}_d + \mathbf{T} + L_1\phi_1(\mathbf{e}_1), \\ \dot{\hat{\mathbf{f}}}_d &= L_2\phi_2(\mathbf{e}_1), \end{aligned} \quad (6)$$

with $\mathbf{e}_1 = \mathbf{z}_1 - \hat{\mathbf{z}}_1$, and $\hat{\mathbf{f}}_d$ is the estimation of \mathbf{f}_d . L_1 and L_2 are the gains to be designed to ensure the stability of the observer, and the functions ϕ_1 and ϕ_2 are given by:

$$\begin{aligned} \phi_1(\mathbf{e}_1) &= k_1[\mathbf{e}_1]^{\frac{1}{2}} + k_1'[\mathbf{e}_1] + k_1''[\mathbf{e}_1]^{\frac{1}{1-d_\infty}}, \\ \phi_2(\mathbf{e}_1) &= k_2[\mathbf{e}_1]^0 + k_2'[\mathbf{e}_1] + k_2''[\mathbf{e}_1]^{\frac{1+d_\infty}{1-d_\infty}}, \end{aligned} \quad (7)$$

where $d_\infty \in (0, 1)$, $k_i > 0$, $k_i' > 0$, $k_i'' > 0$, $i = (1, 2)$. Note that $\phi_1(\mathbf{e}_1)$ and $\phi_2(\mathbf{e}_1)$ are bi-homogeneous, with the degree of homogeneity at the 0-limit being -1 and at the ∞ -limit being d_∞ . The comprehensive definition of bi-homogeneity can refer to [26] and [28].

Subtracting (6) from (5) yields the following error dynamics

$$\begin{aligned} \dot{e}_1 &= -L_1(\phi_1(e_1) - e_2), \\ \dot{e}_2 &= -\frac{L_2}{L_1} \left(\phi_2(e_1) - \frac{\dot{f}_d}{L_2} \right), \end{aligned} \quad (8)$$

with $e_2 = (f_d - \hat{f}_d)/L_1$.

The main result of the FxTDO is summarized in the following theorem.

Theorem 1: For system (5) with Assumption 1, select $0 < d_\infty < 1$ and choose arbitrary positive gains $k_i > 0, k'_i > 0, k''_i > 0$ for $i = 1, 2$. Then, there exist appropriate gains L_1 as specified in (20) and L_2 satisfying

$$L_2 > \bar{\delta}/k_2, \quad (9)$$

such that the observer error dynamics given in (8) are fixed-time stable, i.e., the observer (6) is able to estimate the lumped disturbance f_d in a fixed time \bar{T} , i.e., $\hat{f}_d = f_d$ for $t > \bar{T}$.

Proof: Consider the bi-homogeneous Lyapunov function derived in [28]

$$V(e) = V_1(e_1, e_2) + V_2(e_2), \quad (10)$$

where the functions V_1 and V_2 are defined as

$$\begin{aligned} V_1(e_1, e_2) &= \beta_0 \left(\frac{2}{p_0} \|e_1\|^{\frac{p_0}{2}} - e_1^\top [\xi] \frac{p_0-2}{2} + \frac{p_0-2}{2} \|\xi\|^{\frac{p_0}{2}} \right) \\ &+ \beta_\infty \left(\frac{1-d_\infty}{p_\infty} \|e_1\|^{\frac{p_\infty}{2}} - e_1^\top [\xi] \frac{p_\infty-1+d_\infty}{1-d_\infty} + \frac{p_\infty-1+d_\infty}{p_\infty} \|\xi\|^{\frac{p_\infty}{2}} \right) \end{aligned} \quad (11)$$

$$V_2(e_2) = \frac{\beta'_0}{p_0} \|e_2\|^{p_0} + \frac{\beta'_\infty}{p_\infty} \|e_2\|^{p_\infty}, \quad (12)$$

with $0 < p_\infty \leq \max\{1, 3(1-d_\infty)/2\}$, $1 < p_0 \leq 2p_\infty/(1-d_\infty)$, and $\beta_0, \beta_\infty, \beta'_0, \beta'_\infty$ being arbitrary positive real numbers. ξ is defined as $\xi = \phi_1^{-1}(e_2)$. According to Young's inequality in [29], it can be concluded that $V_1(e_1, e_2) \geq 0$, which ensures the positive definiteness of Lyapunov function $V(e)$ in (10).

The derivative of $V(e)$ along system (8) can be written as

$$\begin{aligned} \dot{V}(e) &= W(e), \\ W(e) &= -g_1 L_1 (\phi_1(e_1) - e_2) - \frac{(g_2 + \sigma_1) L_2}{L_1} \left(\phi_2(e_1) - \frac{\dot{f}_d}{L_2} \right), \end{aligned} \quad (13)$$

where

$$\begin{aligned} g_1 &= \beta_0 \left(e_1^\top \|e_1\|^{\frac{p_0-4}{2}} - \xi^\top \|\xi\|^{\frac{p_0-4}{2}} \right) \\ &+ \beta_\infty \left(e_1^\top \|e_1\|^{\frac{p_\infty-2}{1-d_\infty}} - \xi^\top \|\xi\|^{\frac{p_\infty-2}{1-d_\infty}} \right), \\ \sigma_1 &= \beta_0 \|\xi\|^{\frac{p_0-4}{2}} \frac{\partial \xi}{\partial e_2} \left(\xi^\top - e_1^\top + \frac{p_0-4}{2} (\xi^\top - \frac{e_1^\top \xi \xi^\top}{\|\xi\|^2}) \right) \\ &+ \beta_\infty \|\xi\|^{\frac{p_\infty-2}{1-d_\infty}} \frac{\partial \xi}{\partial e_2} (\xi^\top - e_1^\top) \\ &+ \beta_\infty \|\xi\|^{\frac{p_\infty-2}{1-d_\infty}} \frac{\partial \xi}{\partial e_2} \left(\frac{p_\infty-2+2d_\infty}{1-d_\infty} (\xi^\top - \frac{e_1^\top \xi \xi^\top}{\|\xi\|^2}) \right), \\ g_2 &= \beta'_0 e_2^\top \|e_2\|^{p_0-2} + \beta'_\infty e_2^\top \|e_2\|^{p_\infty-2}. \end{aligned} \quad (14) \quad (15) \quad (16)$$

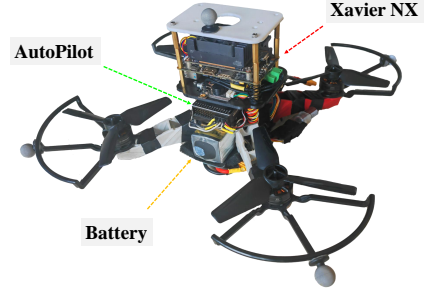


Fig. 4. The quadrotor used for real-world experiments.

Now, we are in the position to demonstrate the negative definiteness of $W(e)$. To this end, consider the structure of $W(e)$, which is restricted to the hypersurfaces

$$\mathbf{Z}_1 = \{\phi_1(e_1) = e_2\}. \quad (17)$$

Note that on the hypersurface \mathbf{Z}_1 , we have $e_1 = \phi_1^{-1}(e_2) = \xi$. Therefore, we can conclude from (14) and (15) that $g_1, \sigma_1 \in \{0\}$ for \mathbf{Z}_1 . Then, let $W_{\mathbf{Z}_1}$ denotes the value of $W(e)$ restricted to the manifold \mathbf{Z}_1 , i.e., by substituting $g_1 = \sigma_1 = 0$ into (13), $W_{\mathbf{Z}_1}$ can be written as

$$\begin{aligned} W_{\mathbf{Z}_1} &= -\frac{g_2 L_2}{L_1} \left(\phi_2(e_1) - \frac{\dot{f}_d}{L_2} \right) \\ &= -\left(\beta'_0 \|e_2\|^{p_0-2} + \beta'_\infty \|e_2\|^{p_\infty-2} \right) * \\ &\frac{L_2}{L_1} e_2^\top \left(k_2 [e_1]^0 + k'_2 [e_1] + k''_2 [e_1]^{\frac{1+d_\infty}{1-d_\infty}} - \frac{\dot{f}_d}{L_2} \right). \end{aligned} \quad (18)$$

Taking into account the properties of the multivariable signum function $x^\top \text{sign}(x) = \|x\|$, and considering that $e_2 = k_1 [e_1]^{\frac{1}{2}} + k'_1 [e_1] + k''_1 [e_1]^{\frac{1+d_\infty}{1-d_\infty}}$ on the hypersurface \mathbf{Z}_1 , with the definition of $W_{\mathbf{Z}_1}^* = \max\{W_{\mathbf{Z}_1}\}$, $W_{\mathbf{Z}_1}^*$ can be expressed as

$$W_{\mathbf{Z}_1}^* = -\left(\beta'_0 \|e_2\|^{p_0-2} + \beta'_\infty \|e_2\|^{p_\infty-2} \right) \frac{L_2}{L_1} \|e_2\| \left(k_2 - \frac{\bar{\delta}}{L_2} \right). \quad (19)$$

Therefore, given that L_2 satisfies the inequality $L_2 > \bar{\delta}/k_2$ in (9), function $W_{\mathbf{Z}_1}^*$ is negative definite. Moreover, from Lemma 1, we can conclude that there exists a positive value of L_1 satisfying

$$\begin{aligned} L_1 &> \max_{(e_1, e_2 \in \mathbb{R}^3)} \{\chi(e_1, e_2)\}, \\ \chi(e_1, e_2) &= \left(\frac{(g_2 + \sigma_1) (\bar{\delta} - L_2 \phi_2(e_1))}{g_1 (\phi_1(e_1) - e_2)} \right)^{\frac{1}{2}}, \end{aligned} \quad (20)$$

such that $W(e)$ is negative definite. Note that $\chi(e_1, e_2)$ is an upper semicontinuous, homogeneous function, and it has a maximum achieved on the homogeneous sphere [30]. Then, according to Lemma 2, the Lyapunov function $V(e)$ satisfies (21) for some positive constants η_0, η_∞ .

$$\dot{V}(e) \leq -\eta_0 V^{\frac{p_0-1}{p_0}}(e) - \eta_\infty V^{\frac{p_\infty+d_\infty}{p_\infty}}(e). \quad (21)$$

Finally, we can obtain the estimation of the fixed convergence time \bar{T}

$$\bar{T} \leq \frac{p_0}{\eta_\infty} \left(\frac{p_\infty}{p_0 d_\infty} + 1 \right) \left(\frac{\eta_0}{\eta_\infty} \right)^{-\frac{1}{\frac{p_\infty}{p_0 d_\infty} + 1}}, \quad (22)$$

which is independent of the initial estimation error [31]. As a result, the fixed-time stable of the observer error dynamics (8) is guaranteed. This completes the proof.

C. Trajectory Tracking Controller Design

To achieve the objective of accurate trajectory tracking in the presence of disturbances, a cascade control strategy is proposed, which is composed of two components: an FxTDO-based MPC controller and an INDI angular velocity controller. The FxTDO-based MPC controller is proposed to track the desired trajectory while simultaneously compensating for the lumped disturbance \mathbf{f}_d . In addition, the INDI angular velocity controller is developed to track the commands generated by the FxTDO-based MPC controller and deal with unknown torque disturbance $\boldsymbol{\tau}_d$.

1) *FxTDO-based MPC controller*: By integrating the estimation of FxTDO into the prediction model, an FxTDO-based MPC controller is developed to achieve robust trajectory tracking of quadrotor. The prediction model employed within the MPC problem is formulated by

$$\dot{\mathbf{p}} = \mathbf{v}, \quad (23a)$$

$$\dot{\mathbf{v}} = -\frac{1}{m} \mathbf{R}_B^W(\mathbf{q}) T_c \mathbf{e}_z^B + \mathbf{g} + \frac{1}{m} \hat{\mathbf{f}}_d, \quad (23b)$$

$$\dot{\mathbf{q}} = \frac{1}{2} \mathbf{q} \otimes \begin{bmatrix} 0 \\ \boldsymbol{\omega}_c \end{bmatrix}, \quad (23c)$$

where $\hat{\mathbf{f}}_d$ is the estimated value of the lumped disturbance provided by FxTDO. During each iteration of solving the MPC problem, the estimated disturbance $\hat{\mathbf{f}}_d$ is assumed to be constant along the prediction horizon.

The controller generates control commands by solving an optimal problem in a receding horizon fashion. To formulate the optimization problem of FxTDO-based MPC controller, the state vector is defined as:

$$\mathbf{x} = [\mathbf{p}, \mathbf{v}, \mathbf{q}]^\top, \quad (24)$$

and control command is defined:

$$\mathbf{u} = [T_c, \boldsymbol{\omega}_c]^\top = [T_c, \omega_{x,c}, \omega_{y,c}, \omega_{z,c}]^\top, \quad (25)$$

where $\boldsymbol{\omega}_c = [\omega_{x,c}, \omega_{y,c}, \omega_{z,c}]^\top$ is the angular velocity command sent to the inner-loop controller.

To formulate the cost function of the optimization problem, which is defined as the cost of states error and control commands error, the reference states and control commands are computed using the concept of differential flatness for quadrotor [32]. For trajectory tracking of quadrotor, position \mathbf{p} and yaw angle ψ are selected to be flat outputs, which means that the desired trajectory $\boldsymbol{\varepsilon}_r$ is defined as $\boldsymbol{\varepsilon}_r = [\mathbf{p}_r, \psi_r]^\top$. The system is discretized into N steps over time horizon T of

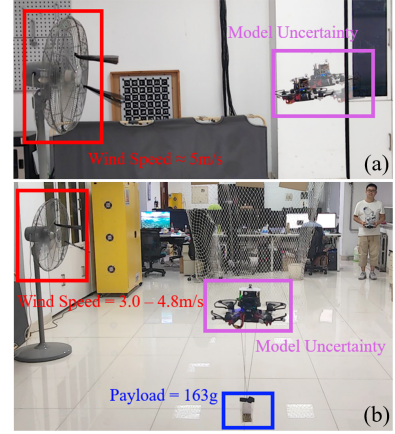


Fig. 5. Disturbances in real-world experiments. (a) Disturbances in hovering tests (*Scenario 1*). (b) Disturbances in trajectory tracking tests (*Scenario 2*).

size $dt = T/N$, yielding a constrained nonlinear optimization problem:

$$\begin{aligned} \min_{\mathbf{u}} \quad & \sum_{k=0}^{N-1} (\Delta \mathbf{x}_k^\top \mathbf{Q} \Delta \mathbf{x}_k + \Delta \mathbf{u}_k^\top \mathbf{R} \Delta \mathbf{u}_k) + \Delta \mathbf{x}_N^\top \mathbf{P} \Delta \mathbf{x}_N \\ \text{s.t.} \quad & \dot{\mathbf{x}} = \mathbf{h}(\mathbf{x}, \mathbf{u}), \mathbf{x}_0 = \mathbf{x}_{init}, \mathbf{u} \in \mathbb{U}, \mathbf{x} \in \mathbb{X}, \mathbf{x}_N \in \mathbb{X}_N \end{aligned} \quad (26)$$

where $\Delta \mathbf{x}_k = \mathbf{x}_k - \mathbf{x}_{k,r}$ and $\Delta \mathbf{u}_k = \mathbf{u}_k - \mathbf{u}_{k,r}$ are respectively the errors of states and control commands, $\mathbf{x}_{k,r}$ and $\mathbf{u}_{k,r}$ are respectively the reference state vector and the reference control command vector computed from the desired trajectory. $\mathbf{Q} \succeq 0$ and $\mathbf{R} \succeq 0$ are positive definite weight matrixes respectively of states error and control commands error, while $\mathbf{P} \succeq 0$ is positive definite weight matrix of terminal states. $\mathbf{h}(\mathbf{x}, \mathbf{u})$ is the prediction model represented in (23). \mathbb{U} , \mathbb{X} and \mathbb{X}_N are constraints of respectively control commands, states and terminal states. The quadratic optimization problem (26) is constructed as a multiple shooting scheme, and a real-time iterative scheme based on the sequential quadratic programming algorithm is employed to solve it. Furthermore, the ACADO [33] toolkit and qpOASES [34] solver are utilized to solve this optimization problem.

In what follows, the proof of the recursive feasibility of the proposed MPC and the stability of the combined system are provided based on the work in [35], [36]. Firstly, for brevity, the optimization problem (26) can be rewritten as the problem of steering the state to the origin in the following:

$$\begin{aligned} V_N^0(\mathbf{x}(k)) = \min_{\mathbf{u}} \quad & \sum_{i=0}^{N-1} l(\mathbf{x}(k+i|k), \mathbf{u}(k+i|k)) \\ & + V_f(\mathbf{x}(k+N|k)), \\ \text{s.t.} \quad & \mathbf{x}(k+i+1|k) = f(\mathbf{x}(k+i|k), \mathbf{u}(k+i|k)), \\ & \mathbf{x}(k+i|k) \in \mathbb{X}, \mathbf{u}(k+i|k) \in \mathbb{U}, \\ & \mathbf{x}(k+N|k) \in \mathbb{X}_N, \mathbf{x}(k|k) = \mathbf{x}(k), \end{aligned} \quad (27)$$

where $f(\mathbf{x}(k+i|k), \mathbf{u}(k+i|k)) = \mathbf{x}(k+i|k) + h(\mathbf{x}(k+i|k), \mathbf{u}(k+i|k)) * dt$. Solving the problem (27) yields the optimal control sequence $\mathbf{u}^*(k) = \{\mathbf{u}^*(k|k), \dots, \mathbf{u}^*(k+N-1|k)\}$. \mathbb{X}_N is assumed to be a closed subset of \mathbb{X} , and the origin is in its interior. Besides, it is assumed that for all $\mathbf{x} \in \mathbb{X}_N$, there exists an implicit control law $\mathbf{u}_N(\mathbf{x}) \in \mathbb{U}$ such that $f(\mathbf{x}, \mathbf{u}_N(\mathbf{x})) \in \mathbb{X}_N$ and $V_f(f(\mathbf{x}, \mathbf{u}_N(\mathbf{x})) \leq V_f(\mathbf{x}) - l(\mathbf{x}, \mathbf{u}_N(\mathbf{x}))$. Additionally, to prove

the recursive feasibility of the proposed MPC, suppose that the optimization problem (27) is feasible at initial time. At time instant k , the optimal control $\mathbf{u}^*(k)$ can steer current state $x(k)$ to the optimal state trajectory $\mathbf{x}^*(k) = \{x^*(k | k), \dots, x^*(k + N | k)\}$ where $x^*(k + N | k) \in \mathbb{X}_N$. At next time instant $k + 1$, a control sequence is constructed by

$$\tilde{\mathbf{u}}(k + 1) = \begin{cases} u^*(k + i | k), & i = 1, \dots, N - 1, \\ u_N(x^*(k + N | k)), & i = N. \end{cases} \quad (28)$$

Using the constructed control sequence (28) at time instant $k + 1$, the state sequence $x(k + i | k + 1), i = 1, \dots, N$ can be obtained, where $x(k + N | k + 1) \in \mathbb{X}_N$. Under the control command $u_N(x^*(k + N | k))$ in (28), the state $x(k + N + 1 | k + 1) = f(x^*(k + N | k), u_N(x^*(k + N | k))) \in \mathbb{X}_N$ is feasible. Therefore, the constructed control sequence (28) is a feasible solution of the proposed MPC at time instant $k + 1$, which means that the recursive feasibility of the proposed MPC is ensured.

Then the stability of the closed-loop system with the proposed MPC is established, with a Lyapunov function candidate defined as $V_N^0(x(k)) = \min_{\mathbf{u}} \sum_{i=0}^{N-1} l(x^*(k + i | k), u^*(k + i | k)) + V_f(x^*(k + N | k))$, at time instant k . Considering the constructed feasible control sequence (28), the Lyapunov function $V_N^0(x(k + 1))$ at next time instant $k + 1$ can be written as

$$\begin{aligned} & V_N^0(x(k + 1)) \\ &= \min_{\mathbf{u}} \sum_{i=0}^{N-1} l(x^*(k + 1 + i | k + 1), u^*(k + 1 + i | k + 1)) \\ &\quad + V_f(x^*(k + 1 + N | k + 1)) \\ &\leq V_N^0(x(k)) - l(x^*(k | k), u^*(k | k)). \end{aligned} \quad (29)$$

Therefore, $V_N^0(x(k + 1)) < V_N^0(x(k))$ holds until the state $x(k)$ converges to zero, and the stability of the closed-loop system with the proposed MPC is established.

2) *INDI Angular Velocity Controller*: To track the angular velocity command ω_c in the presence of unknown torque disturbance τ_d , an INDI angular velocity controller is employed in this section [12]. Consider quadrotor dynamics (1d), which can be rewritten as the following expression:

$$\tau_d = \mathbf{J}\dot{\omega}_f - \tau_{c,f} + \omega_f \times \mathbf{J}\omega_f, \quad (30)$$

where $\dot{\omega}_f$ is the feedback angular acceleration, $\tau_{c,f}$ is the torque command from the last computation, and ω_f represents the feedback angular velocity. Substituting (30) into (1d) yields:

$$\begin{aligned} \dot{\omega} &= \mathbf{J}^{-1}[\tau_c - \omega \times \mathbf{J}\omega] + \mathbf{J}^{-1}\tau_d \\ &= \mathbf{J}^{-1}[\tau_c - \omega \times \mathbf{J}\omega + (\mathbf{J}\dot{\omega}_f - \tau_{c,f} + \omega_f \times \mathbf{J}\omega_f)] \\ &= \dot{\omega}_f + \mathbf{J}^{-1}[\tau_c - \tau_{c,f}], \end{aligned} \quad (31)$$

where it is supposed that $\omega \times \mathbf{J}\omega = \omega_f \times \mathbf{J}\omega_f$, since this term is regarded as relatively slow-changing in comparison to the angular acceleration $\dot{\omega}$ and the torque command τ [12], [13]. Then, the control command τ_c can be calculated by

$$\tau_c = \tau_{c,f} + \mathbf{J}(\dot{\omega}_c - \dot{\omega}_f), \quad (32)$$

where $\dot{\omega}_c$ is the virtual angular acceleration command which can be derived from the following proportional controller:

$$\dot{\omega}_c = \mathbf{K}_\omega(\omega_c - \omega_f) + \dot{\omega}_r, \quad (33)$$

where ω_c is the reference angular velocity that comes from the control command of the FxTDO-based MPC controller, and $\dot{\omega}_r$ represents the reference angular acceleration.

Remark 1: In the real-world quadrotor platform, control commands sent to quadrotor need to be computed at a very high frequency, such as 1000 Hz [12]. However, the excessive computational time required of MPC on the onboard computer poses a limitation on its applicability within the inner-loop. Therefore, it is necessary to incorporate an inner-loop controller with lower computational requirements. Considering the advantages of INDI method, including the low computational requirements and sufficient robustness [12], [37], an INDI angular velocity controller is employed as the inner-loop controller.

IV. SIMULATION AND EXPERIMENT

In this section, simulations in Gazebo and real-world experiments are developed to evaluate the effectiveness of the proposed method. For brevity, the proposed method is denoted as FxTDO-MPC & INDI. To highlight the effectiveness of the proposed method, a conventional PID controller, a conventional MPC controller, a robust tube-based MPC (RT-MPC) controller [38] and a high-gain disturbance observer-based MPC (HGDO-MPC) controller [39] are employed for comparison, incorporating with inner-loop INDI angular velocity controller. The MPC, RT-MPC and HGDO-MPC methods adopt the same set of parameters as the FxTDO-MPC method, while the PID controller is carefully tuned for optimal performance. Notably, the RT-MPC framework proposed in [38] is designed for linear systems. To adopt the RT-MPC method for quadrotor, several modifications are implemented as follows. Firstly, the nominal MPC controller within the RT-MPC framework is constructed based on a nonlinear model regardless of disturbances, generating optimal control sequence $\mathbf{u}_n^*(k) = \{\mathbf{u}_n^*(k | k), \dots, \mathbf{u}_n^*(k + N - 1 | k)\}$ and the nominal optimal state sequence $\mathbf{x}^*(k) = \{\mathbf{x}^*(k | k), \dots, \mathbf{x}^*(k + N | k)\}$. Furthermore, this nominal MPC controller utilizes the control sequence and the initial state as decision variables [38], [40]. Secondly, the quadrotor model is linearized into the discrete-time form: $\mathbf{x}_{k+1} = \mathbf{A}\mathbf{x}_k + \mathbf{B}\mathbf{u}_k$, and the feedback control law is defined: $\mathbf{u}_{f,k} = \mathbf{K}(\mathbf{x}_k - \mathbf{x}^*(k | k))$, where the gain matrix \mathbf{K} is obtained by solving the associated Riccati equation, ensuring that $\mathbf{A}_K := \mathbf{A} + \mathbf{B}\mathbf{K}$ is stable [38], [40]. Finally, by combining the nominal MPC controller and the feedback controller, the control command of RT-MPC \mathbf{u}_k is computed as: $\mathbf{u}_k = \mathbf{u}_n^*(k | k) + \mathbf{K}(\mathbf{x}_k - \mathbf{x}^*(k | k))$. On the other hand, an HGDO-MPC method is constructed by replacing FxTDO in the proposed FxTDO-MPC method with a multivariable HGDO. The HGDO takes the form: $\dot{\hat{\mathbf{z}}}_1 = \hat{\mathbf{z}}_2 + \mathbf{T} + \frac{\alpha_1}{\varepsilon}\mathbf{e}_1$, $\dot{\mathbf{f}}_d = \frac{\alpha_2}{\varepsilon^2}\mathbf{e}_1$, where α_1 , α_2 , and ε are positive constants [39].

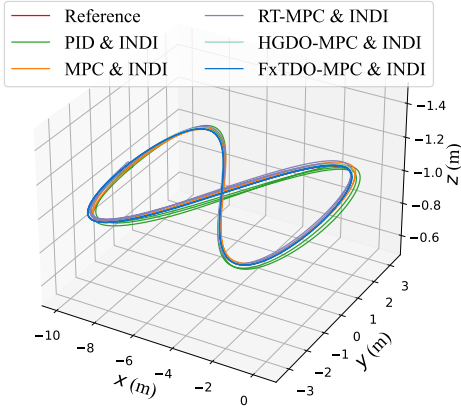


Fig. 6. Quadrotor 3D trajectory tracking performance in Simulation.

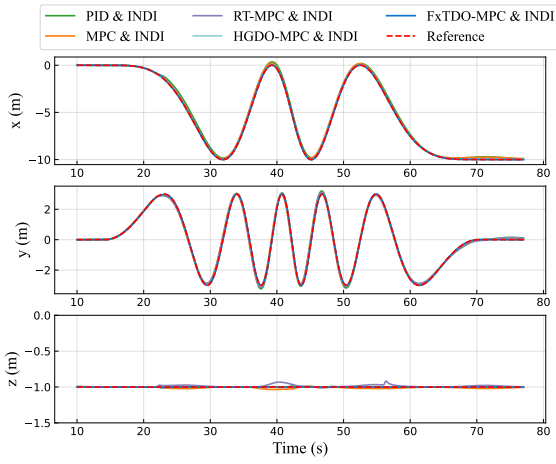


Fig. 7. Position tracking performance in Simulation.

A. Simulation Setups

The proposed controller is executed in the ROS environment and sends control command (T_c, τ_c) to quadrotor, which runs in Gazebo. The FxTDO-based MPC controller runs at 100 Hz while the INDI angular velocity controller operates at 1000 Hz. The model configurations for quadrotor in Gazebo are shown in Table I. The gains of the proposed controller and disturbance observer are summarized in Table II.

In this scenario, a set of flight tests in simulation is developed to prove the effectiveness of the proposed controller and FxTDO. The desired trajectories ε_r considered here are the eight-shaped trajectories as shown in Fig. 1, which is defined as:

$$\varepsilon_r = [p_r, \psi_r]^T = \begin{bmatrix} r_x \sin k_t t^2 \cos k_t t^2 \\ r_y \cos k_t t^2 - r_y \\ r_z \\ 0 \end{bmatrix}, \quad (34)$$

with $r_x = 3$ m, $r_y = 5$ m, $r_z = -1$ m and $k_t = 0.01$. In the simulation, the complex disturbance effects f_d and τ_d are defined:

$$f_d = \begin{bmatrix} 1 + 0.5 \sin \frac{2\pi \Delta t}{15} \\ -0.5 \cos \frac{2\pi \Delta t}{15} \\ 0 \end{bmatrix}, \quad \tau_d = \begin{bmatrix} 0.2 \sin \frac{2\pi \Delta t}{15} \\ 0.2 \cos \frac{2\pi \Delta t}{15} \\ 0 \end{bmatrix}, \quad (35)$$

where Δt is the start time of injecting disturbances.

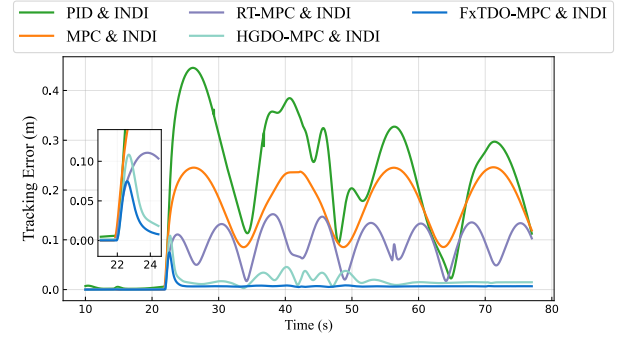


Fig. 8. Position tracking error in Simulation.

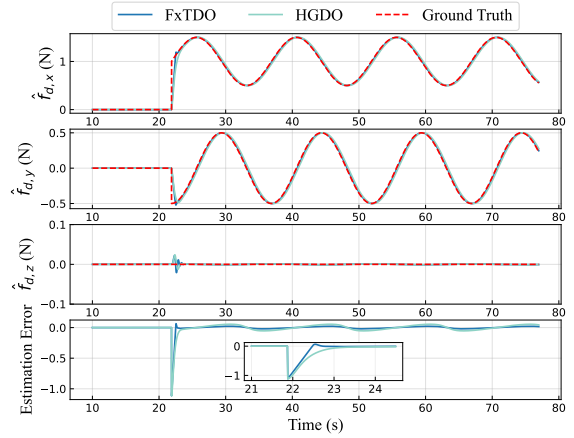


Fig. 9. The disturbance estimation in Simulation.

B. Simulation Results

The trajectory tracking performance in the influence of external disturbances (35) is depicted in Figs. 6 and 7, illustrating that the proposed method effectively enables the quadrotor to track the desired trajectory in the presence of disturbances. The position tracking error is presented in Fig. 8, with corresponding Root Mean Squared Errors (RMSE) of 0.245 m, 0.169 m, 0.092 m (RT-MPC & INDI), 0.020 m (HGDO-MPC & INDI), and 0.009 m (FxTDO-MPC & INDI), respectively. It can be seen from Fig. 8 that the proposed FxTDO-MPC & INDI method achieves the lowest tracking error compared to the other methods. The disturbance estimation using two disturbance observers is depicted in Fig. 9, illustrating that the proposed FxTDO converges within about 0.94 seconds. It is obvious that the proposed FxTDO achieves a faster convergence rate compared to the HGDO. The faster convergence of the FxTDO allows for quicker adjustments in the control inputs, leading to improved tracking performance, as illustrated in Fig. 8. Therefore, when subjected to disturbances, the method utilizing the proposed FxTDO exhibits a more rapid decrease in the position tracking error compared to the method employing the HGDO. Consequently, employing a disturbance observer with faster convergence properties in observer-based MPC scheme results in smaller transient error. In addition, to further validate the robust performance of the proposed method, Monte Carlo simulations are conducted by multiplying the disturbance f_d in (35) by a random

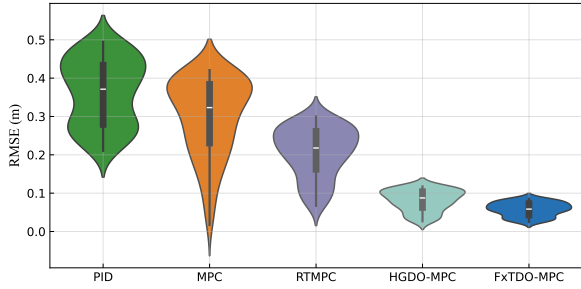


Fig. 10. The distribution of position tracking RMSE of Monte Carlo simulations.

TABLE I
QUADROTOR CONFIGURATIONS IN SIMULATION

Parameters	Values	Parameters	Values
m	1.0 kg	l	0.17 m
J_x	$2.64 \times 10^{-3} \text{ kg}\cdot\text{m}^2$	d_x	$9.4 \times 10^{-9} \text{ m}$
J_y	$2.64 \times 10^{-3} \text{ kg}\cdot\text{m}^2$	d_y	$9.4 \times 10^{-9} \text{ m}$
J_z	$4.96 \times 10^{-3} \text{ kg}\cdot\text{m}^2$	c_T	$2.5 \times 10^{-9} \text{ m}$

$k \in [0, 1]$. Notably, the simulations are executed 500 times for all methods. The distribution of position tracking RMSE is summarized in Fig. 10. It is obvious that the proposed method demonstrates the lowest error level with a concentrated error distribution, indicating the ability to ensure the robust performance of system in the presence of varying degrees of disturbances.

C. Real-world Experiment Setups

To further verify the performance of the proposed method, a real quadrotor platform, as depicted in Fig. 4, has been employed. The platform has a weight of 1.05 kg, with a thrust-to-weight ratio of 4:1. The inertia matrix $\mathbf{J} = \text{diag}(0.0235, 0.0219, 0.0285) \text{ kgm}^2$ is roughly estimated through the bifilar pendulum experiment. The FxTDO-MPC algorithm runs on a Jetson Xavier NX onboard computer, computing the collective thrust and angular velocity. The computational time for each time step of the MPC on onboard com-

TABLE II
THE PARAMETER VALUES OF THE ADOPTED METHOD.

Methods	Parameters	Values
MPC	$\mathbf{Q}_p / \mathbf{P}_p$	$\text{diag}(1500, 1500, 1500)$
	$\mathbf{Q}_v / \mathbf{P}_v$	$\text{diag}(400, 400, 400)$
	$\mathbf{Q}_q / \mathbf{P}_q$	$\text{diag}(500, 500, 500, 500)$
	\mathbf{R}	$\text{diag}(1, 10, 10, 10)$
	N	10
	dt	100 ms
INDI	\mathbf{K}_ω	$\text{diag}(400, 400, 300)$
FxTDO	k_i	2.0
	k'_i	0.6
	k''_i	3.0
	d_∞	1/3
	L_1, L_2	1.0
HGDO	α_1	3.0
	α_2	2.0
	ε	0.2

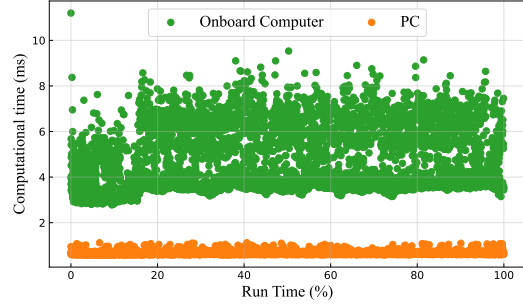


Fig. 11. The computational time of the the proposed FxTDO-MPC method.

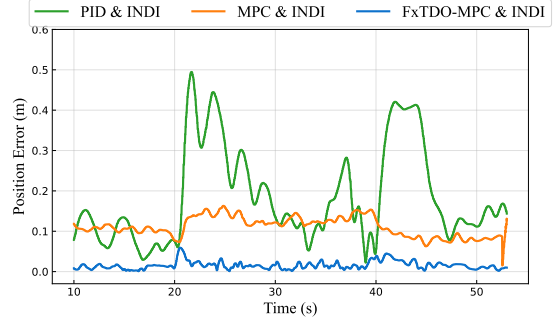


Fig. 12. Position error in *Scenario 1*.

puter and PC is depicted in Fig. 11, where the PC is equipped with an Intel Core i9-11900, an NVIDIA GeForce RTX 3070 and 32G RAM. The INDI angular velocity controller operates on a CUAV v5+ autopilot running the PX4 firmware. The gains and parameters used in real-world experiments are the same as those in Table II. All real-world flight experiments are performed under the Optitrack motion capture system. In addition, the PX4 firmware provides the extended Kalman filter for state estimation which fuses Inertial Measurement Unit (IMU) data with pose information from Optitrack. Two experiment scenarios with disturbances are tested: 1) *Hovering performance with persistent wind disturbance (Scenario 1)*; 2) *Trajectory tracking with complex disturbances (Scenario 2)*.

D. Real-world Experiment Results

1) *Hover performance with persistent wind disturbance (Scenario 1)*: In this scenario, a quadrotor hovers in a fixed position. Persistent wind gusts are generated by an electric fan. The wind speed is measured using an anemometer in the position where the quadrotor hovers, which is about 5.0 m/s, as shown in Fig. 5. The quadrotor platform exhibits model uncertainty primarily due to the inaccurate inertia matrix. The position error and RMSE are summarized in Fig. 12 and Table III. From these results, it can be seen that the proposed method achieves a remarkably high level of control accuracy, leading to a large reduction in RMSE compared to the MPC without FxTDO and classical PID controller. The results of the FxTDO are provided in Fig. 13. The electric fan is activated at around 20 seconds, and it can be observed that the proposed FxTDO is able to quickly estimate the disturbance mainly caused by the electric fan.

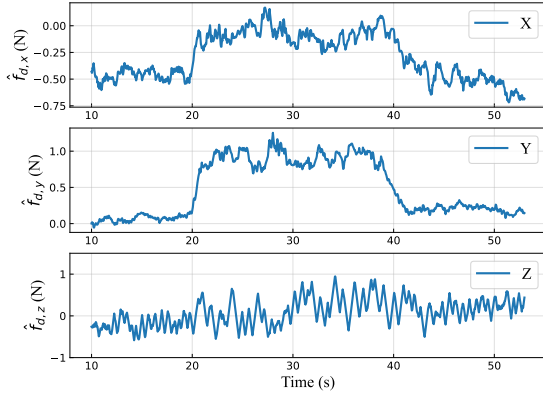


Fig. 13. The disturbance estimation in *Scenario 1*.

TABLE III
THE POSITION TRACKING RMSE COMPARISON IN REAL-WORLD
EXPERIMENTS (SCENARIO 1 AND SCENARIO 2).

Methods	RMSE (m)	
	<i>Scenario 1</i>	<i>Scenario 2</i>
PID & INDI	0.219	0.302
MPC & INDI	0.113	0.178
FxTDO-MPC & INDI	0.018	0.051

2) *Trajectory tracking with complex disturbances (Scenario 2)*: In order to assess the efficiency of the proposed algorithm in the presence of complex disturbances, a payload with a mass of 163 g is affixed to the quadrotor, while wind disturbance with speed ranging from 3.0 m/s to 4.8 m/s is introduced in the center of the experimental site, as shown in Fig. 5. Due to the limited space in the indoor environment, the desired trajectory defined in (34) with $r_x = 1.2$ m, $r_y = 2.4$ m, $r_z = 1.0$ m and $k_t = 0.01$ is used. Figs. 14 and 15 illustrate the trajectory tracking performance under three different methods. Furthermore, the tracking error can be found in Fig. 16 and Table III, where the proposed method achieves 72% and 83% decrease in RMSE compared to MPC & INDI and PID & INDI respectively. From the position error in Fig. 16 and RMSE in Table III, it can be concluded that the

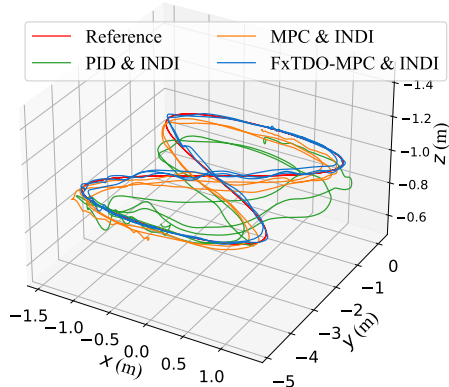


Fig. 14. Quadrotor 3D trajectory tracking performance in *Scenario 2*.

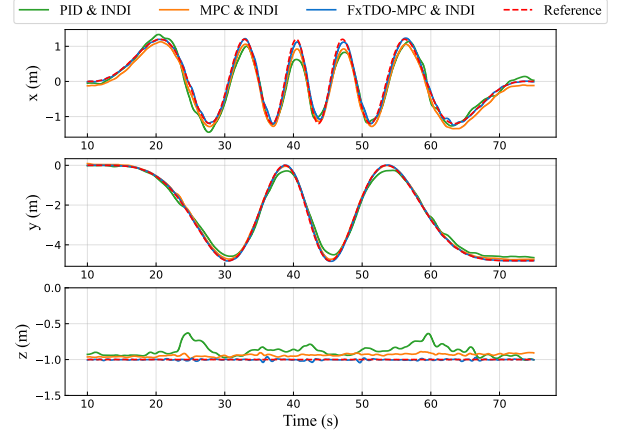


Fig. 15. Position tracking performance in *Scenario 2*.

proposed approach achieves accurate trajectory tracking while effectively rejecting complex disturbances. Fig. 17 presents the estimated value of FxTDO in *Scenario 2*, which includes the complex influence of swaying load, electric fan, model uncertainty, and aerodynamic drag force during flight. For $\hat{f}_{d,x}$ and $\hat{f}_{d,y}$ in *Scenario 2*, the primary source of disturbance is the electric fan and aerodynamic drag force which is related to the velocity of quadrotor [13]. The blue line in Fig. 17 represents the estimated value of FxTDO, while the red dashed line represents the velocity of quadrotor. Although these two variables do not exhibit a linear correlation, they demonstrate a consistent similarity in the overall pattern of change. It should be noted that the green dashed line represents the force caused by the payload, and the estimated value $\hat{f}_{d,z}$ demonstrates fluctuation around the green dashed line, which is attributed to the swaying motion of the payload.

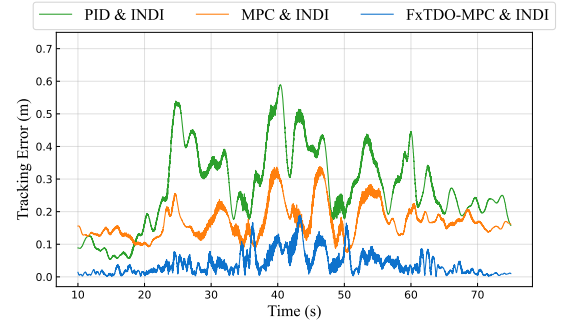


Fig. 16. Position tracking error in *Scenario 2*.

V. CONCLUSION

This paper proposes an FxTDO-MPC algorithm for robust trajectory tracking of quadrotor in the presence of disturbances. Firstly, the FxTDO is introduced to estimate the lumped disturbances. The convergence of estimation error within a fixed convergence time is guaranteed by the bi-limit homogeneity and Lyapunov techniques. Then, the observer-based model predictive controller is formulated by integrating the estimation of FxTDO into the prediction model. The proposed method achieves accurate trajectory tracking and robust

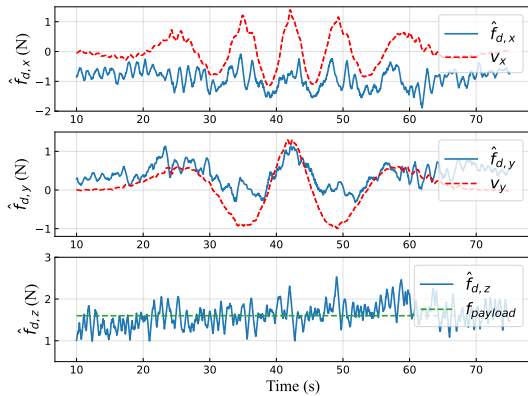


Fig. 17. The disturbance estimation in *Scenario 2*.

disturbance rejection of quadrotor, while simulations and real-world experiments are developed to evaluate the effectiveness of the proposed method. Future work will focus on extending the proposed method to various vehicle models, such as fixed-wing UAVs, and to diverse operational environments, such as scenarios involving actuator failures.

REFERENCES

- [1] Y. Li, G. Lu, D. He, and F. Zhang, "Robocentric model-based visual servoing for quadrotor flights," *IEEE/ASME Transactions on Mechatronics*, vol. 28, no. 4, pp. 2155–2166, 2023.
- [2] H. H. Kang, D. K. Lee, and C. K. Ahn, "Finite-memory-structured online training algorithm for system identification of unmanned aerial vehicles with neural networks," *IEEE/ASME Transactions on Mechatronics*, vol. 27, no. 6, pp. 5846–5856, 2022.
- [3] S. Bouabdallah, A. Noth, and R. Siegwart, "Pid vs lqr control techniques applied to an indoor micro quadrotor," in *2004 IEEE/RSJ International Conference on Intelligent Robots and Systems (IROS)*(IEEE Cat. No. 04CH37566), vol. 3. IEEE, 2004, pp. 2451–2456.
- [4] A. Tayebi and S. McGilvray, "Attitude stabilization of a vtol quadrotor aircraft," *IEEE Transactions on control systems technology*, vol. 14, no. 3, pp. 562–571, 2006.
- [5] S. Khatoun, D. Gupta, and L. Das, "Pid & lqr control for a quadrotor: Modeling and simulation," in *2014 international conference on advances in computing, communications and informatics (ICACCI)*. IEEE, 2014, pp. 796–802.
- [6] A. Dharmawan, T. K. Priyambodo *et al.*, "Model of linear quadratic regulator (lqr) control method in hovering state of quadrotor," *Journal of Telecommunication, Electronic and Computer Engineering (JTEC)*, vol. 9, no. 3, pp. 135–143, 2017.
- [7] B. Tian, J. Cui, H. Lu, Z. Zuo, and Q. Zong, "Adaptive finite-time attitude tracking of quadrotors with experiments and comparisons," *IEEE Transactions on Industrial Electronics*, vol. 66, no. 12, pp. 9428–9438, 2019.
- [8] B. Tian, J. Cui, H. Lu, L. Liu, and Q. Zong, "Attitude control of uavs based on event-triggered supertwisting algorithm," *IEEE Transactions on Industrial Informatics*, vol. 17, no. 2, pp. 1029–1038, 2020.
- [9] B. Zhao, B. Xian, Y. Zhang, and X. Zhang, "Nonlinear robust adaptive tracking control of a quadrotor uav via immersion and invariance methodology," *IEEE Transactions on Industrial Electronics*, vol. 62, no. 5, pp. 2891–2902, 2014.
- [10] T. Madani and A. Benallegue, "Backstepping control for a quadrotor helicopter," in *2006 IEEE/RSJ International Conference on Intelligent Robots and Systems*. IEEE, 2006, pp. 3255–3260.
- [11] N. Guenard, T. Hamel, and R. Mahony, "A practical visual servo control for an unmanned aerial vehicle," *IEEE Transactions on Robotics*, vol. 24, no. 2, pp. 331–340, 2008.
- [12] E. Tal and S. Karaman, "Accurate tracking of aggressive quadrotor trajectories using incremental nonlinear dynamic inversion and differential flatness," *IEEE Transactions on Control Systems Technology*, vol. 29, no. 3, pp. 1203–1218, 2020.
- [13] S. Sun, A. Romero, P. Foehn, E. Kaufmann, and D. Scaramuzza, "A comparative study of nonlinear mpc and differential-flatness-based control for quadrotor agile flight," *IEEE Transactions on Robotics*, vol. 38, no. 6, pp. 3357–3373, 2022.
- [14] H. Hangxuan and D. Haibin, "A multi-strategy pigeon-inspired optimization approach to active disturbance rejection control parameters tuning for vertical take-off and landing fixed-wing uav," *Chinese Journal of Aeronautics*, vol. 35, no. 1, pp. 19–30, 2022.
- [15] X. Zhang, Y. Wang, G. Zhu, X. Chen, and C.-Y. Su, "Discrete-time adaptive neural tracking control and its experiments for quadrotor unmanned aerial vehicle systems," *IEEE/ASME Transactions on Mechatronics*, vol. 28, no. 3, pp. 1201–1212, 2023.
- [16] M. Kamel, M. Burri, and R. Siegwart, "Linear vs nonlinear mpc for trajectory tracking applied to rotary wing micro aerial vehicles," *IFAC-PapersOnLine*, vol. 50, no. 1, pp. 3463–3469, 2017.
- [17] D. Hentzen, T. Stastny, R. Siegwart, and R. Brockers, "Disturbance estimation and rejection for high-precision multirotor position control," in *2019 IEEE/RSJ International Conference on Intelligent Robots and Systems (IROS)*. IEEE, 2019, pp. 2797–2804.
- [18] G. Torrente, E. Kaufmann, P. Föhn, and D. Scaramuzza, "Data-driven mpc for quadrotors," *IEEE Robotics and Automation Letters*, vol. 6, no. 2, pp. 3769–3776, 2021.
- [19] T. Salzmann, E. Kaufmann, J. Arrizabalaga, M. Pavone, D. Scaramuzza, and M. Ryll, "Real-time neural mpc: Deep learning model predictive control for quadrotors and agile robotic platforms," *IEEE Robotics and Automation Letters*, vol. 8, no. 4, pp. 2397–2404, 2023.
- [20] A. Saviolo, G. Li, and G. Loianno, "Physics-inspired temporal learning of quadrotor dynamics for accurate model predictive trajectory tracking," *IEEE Robotics and Automation Letters*, vol. 7, no. 4, pp. 10256–10263, 2022.
- [21] Y. Zhang, C. Edwards, M. Belmont, and G. Li, "Robust model predictive control for constrained linear system based on a sliding mode disturbance observer," *Automatica*, vol. 154, p. 111101, 2023.
- [22] É. L. Oliveira, R. M. Orsino, and D. C. Donha, "Disturbance-observer-based model predictive control of underwater vehicle manipulator systems," *IFAC-PapersOnLine*, vol. 54, no. 16, pp. 348–355, 2021.
- [23] Y. Yan, J. Yang, Z. Sun, S. Li, and H. Yu, "Non-linear-disturbance-observer-enhanced mpc for motion control systems with multiple disturbances," *IET Control Theory & Applications*, vol. 14, no. 1, pp. 63–72, 2020.
- [24] M. S. Mousavi, S. A. Davari, V. Nekoukar, C. Garcia, and J. Rodriguez, "Integral sliding mode observer-based ultralocal model for finite-set model predictive current control of induction motor," *IEEE Journal of Emerging and Selected Topics in Power Electronics*, vol. 10, no. 3, pp. 2912–2922, 2021.
- [25] Cruz-Zavala, Emmanuel and Moreno, Jaime A, "High-order sliding-mode control design homogeneous in the bi-limit," *International Journal of Robust and Nonlinear Control*, vol. 31, no. 9, pp. 3380–3416, 2021.
- [26] V. Andrieu, L. Praly, and A. Astolfi, "Homogeneous approximation, recursive observer design, and output feedback," *SIAM Journal on control and optimization*, vol. 47, no. 4, pp. 1814–1850, 2008.
- [27] B. Tian, Z. Zuo, X. Yan, and H. Wang, "A fixed-time output feedback control scheme for double integrator systems," *Automatica*, vol. 80, pp. 17–24, 2017.
- [28] J. A. Moreno, "Arbitrary-order fixed-time differentiators," *IEEE Transactions on Automatic Control*, vol. 67, no. 3, pp. 1543–1549, 2021.
- [29] G. H. Hardy, J. E. Littlewood, and G. Pólya, *Inequalities*. Cambridge university press, 1952.
- [30] E. Cruz-Zavala and J. A. Moreno, "Lyapunov functions for continuous and discontinuous differentiators," *IFAC-PapersOnLine*, vol. 49, no. 18, pp. 660–665, 2016.
- [31] A. Polyakov, "Nonlinear feedback design for fixed-time stabilization of linear control systems," *IEEE transactions on Automatic Control*, vol. 57, no. 8, pp. 2106–2110, 2011.
- [32] D. Mellinger and V. Kumar, "Minimum snap trajectory generation and control for quadrotors," in *2011 IEEE international conference on robotics and automation*. IEEE, 2011, pp. 2520–2525.
- [33] R. Quirynen, B. Houska, M. Vallerio, D. Telen, F. Logist, J. Van Impe, and M. Diehl, "Symmetric algorithmic differentiation based exact hessian sqp method and software for economic mpc," in *53rd IEEE Conference on Decision and Control*. IEEE, 2014, pp. 2752–2757.
- [34] H. J. Ferreau, C. Kirches, A. Potschka, H. G. Bock, and M. Diehl, "qpOases: A parametric active-set algorithm for quadratic programming," *Mathematical Programming Computation*, vol. 6, pp. 327–363, 2014.
- [35] D. Q. Mayne, J. B. Rawlings, C. V. Rao, and P. O. Scokaert, "Constrained model predictive control: Stability and optimality," *Automatica*, vol. 36, no. 6, pp. 789–814, 2000.

- [36] X. Fang and W.-H. Chen, "Model predictive control with preview: Recursive feasibility and stability," *IEEE Control Systems Letters*, vol. 6, pp. 2647–2652, 2022.
- [37] H. Li, H. Wang, C. Feng, F. Gao, B. Zhou, and S. Shen, "Autotrans: A complete planning and control framework for autonomous uav payload transportation," *IEEE Robotics and Automation Letters*, vol. 8, no. 10, pp. 6859–6866, 2023.
- [38] D. Q. Mayne, M. M. Seron, and S. V. Raković, "Robust model predictive control of constrained linear systems with bounded disturbances," *Automatica*, vol. 41, no. 2, pp. 219–224, 2005.
- [39] H. K. Khalil and L. Praly, "High-gain observers in nonlinear feedback control," *International Journal of Robust and Nonlinear Control*, vol. 24, no. 6, pp. 993–1015, 2014.
- [40] M. Mammarella and E. Capello, "Tube-based robust mpc processor-in-the-loop validation for fixed-wing uavs," *Journal of Intelligent & Robotic Systems*, vol. 100, no. 1, pp. 239–258, 2020.